



POLİTEKNİK DERGİSİ

JOURNAL of POLYTECHNIC

ISSN: 1302-0900 (PRINT), ISSN: 2147-9429 (ONLINE)

URL: <http://dergipark.org.tr/politeknik>



Investigation of turbulent flow around circular high-rise structure with various balcony design

Çeşitli balkon tasarımlarına sahip dairesel kesitli yüksek binalar etrafındaki türbülanslı akışın incelenmesi

Yazar(lar) (Author(s)): Aleyna AĞIRMAN KALCA¹, Tekmile CÜREBAL², Yücel ÖZMEN³

ORCID¹: 0000-0002-1147-141x

ORCID²: 0000-0002-9156-5917

ORCID³: 0000-0003-1127-1060

To cite to this article: Ağırman Kalca A., Cürebal T. and Özmen Y., “Investigation of turbulent flow around circular high-rise structure with various balcony design”, *Journal of Polytechnic*, *(*) : *, (*).

Bu makaleye şu şekilde atıfta bulunabilirsiniz: Ağırman Kalca A., Cürebal T. ve Özmen Y., “Investigation of turbulent flow around circular high-rise structure with various balcony design”, *Politeknik Dergisi*, *(*) : *, (*).

Erişim linki (To link to this article): <http://dergipark.org.tr/politeknik/archive>

DOI: 10.2339/politeknik.1492090

Investigation of Turbulent Flow Around Circular High-Rise Structure with Various Balcony Design

Highlights

- ❖ Investigation of flow patterns in models with and without balconies
- ❖ Effect of different balcony heights and diameters on pressure coefficient
- ❖ Effect of different balcony heights and diameters on velocity distribution
- ❖ Numerical simulations using the Realizable $k-\epsilon$ model
- ❖ Experimental flow visualization using the smoke-wire technique

Graphical Abstract

For all balcony diameters, the most critical pressure coefficient values calculated on this surface are determined as an approximately -0.35 . This indicates that the leeward region is less critical in terms of suction effect compared to the windward region. The findings reveal that the model with a balcony diameter of $d_2=35$ mm is more effective in improving the critical suction effect.

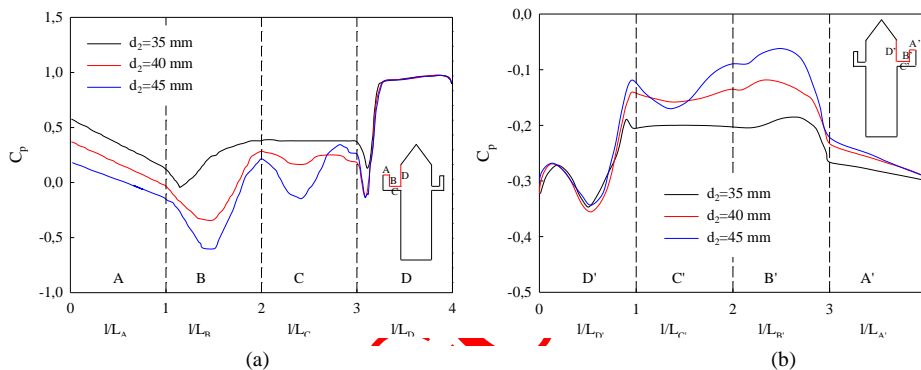


Figure. Variation of the pressure distributions calculated on the balcony surfaces along the middle axis of the model for three different balcony diameters (a) windward region, (b) leeward region

Aim

This study examines the velocity distributions around circular cross-sectioned high-rise structure with and without balconies, aiming to obtain average pressure coefficients along the balcony surfaces based on balcony position and diameter.

Design & Methodology

In the experimental part of the study, the flow visualization around the model placed in the wind tunnel test section was achieved using the smoke-wire technique. In the numerical part, the flow patterns around the models, velocity distributions, and pressure coefficients on the balcony surfaces are calculated using the Realizable $k-\epsilon$ turbulence model.

Originality

This study mainly focuses on examining the velocity distributions around circular cross-sectioned high-rise structures with and without balconies, aiming to obtain average pressure coefficients based on balcony position and diameter.

Findings

Taking into consideration the pressure distributions calculated on all balcony surfaces in the windward region, it is revealed that the best performance is reached in the $h/d_1=3$ case.

Conclusion

The maximum pressure coefficient values are achieved for $h/d_1=3$, and the minimum pressure coefficient values are observed for $h/d_1=4$ on all balcony surfaces in the windward and leeward regions.

Declaration of Ethical Standards

The author(s) of this article declare that the materials and methods used in this study do not require ethical committee permission and/or legal-special permission.

Investigation of Turbulent Flow Around Circular High-Rise Structure with Various Balcony Design

Araştırma Makalesi / Research Article

Aleyna AĞIRMAN KALCA¹, Tekmile CÜREBAL^{1*}, Yücel ÖZMEN¹

¹ Karadeniz Technical University, Faculty of Engineering, Department of Mechanical Engineering, Trabzon, 61080, Türkiye
(Geliş/Received : 30.05.2024 ; Kabul/Accepted : 14.01.2025 ; Erken Görünüm/Early View : 19.03.2025)

ABSTRACT

In this study, flow fields around circular cross-sectioned high-rise structures with and without balconies have been investigated. Three different balcony heights ($h/d_1=3$, $h/d_1=3.5$, $h/d_1=4$) and three different balcony diameters (35 mm, 40 mm, 45 mm) were considered in the study, with the experiments carried out at a free stream velocity of 15 m/s. In the experimental part of the study, flow visualization around the model ($h/d_1=3.5$) was achieved using the smoke-wire technique in the wind tunnel test section. In the numerical part, the flow patterns around the models, velocity distributions, and pressure coefficients on the balcony surfaces are calculated using the Realizable $k-\epsilon$ turbulence model. The pressure coefficient distributions are directly affected by the position of different balcony heights. When different balcony heights are compared, it is seen that the highest pressure coefficient values are achieved for $h/d_1=3$, while the most critical pressure coefficient values are obtained in the case of $h/d_1=4$.

Keywords: Balcony height, computational fluid dynamics (CFD), cylindrical building, pressure coefficient, wind tunnel.

Çeşitli Balkon Tasarımlarına Sahip Dairesel Kesitli Yüksek Binalar Etrafındaki Türbülanslı Akışın İncelenmesi

ÖZ

Bu çalışmada, balkonlu ve balkonsuz dairesel kesitli yüksek binaların etrafındaki akış alanları incelenmiştir. Çalışmada üç farklı balkon yüksekliği ($h/d_1=3$, $h/d_1=3.5$, $h/d_1=4$) ve üç farklı balkon çapı (35 mm, 40 mm, 45 mm) dikkate alınmış olup, deneyler 15 m/s serbest akış hızında gerçekleştirilmiştir. Çalışmanın deneysel kısmında, rüzgar tüneli test bölgesine yerleştirilen model etrafındaki ($h/d_1=3.5$) akış görüntülemesi duman teli tekniği kullanılarak gerçekleştirilmiştir. Sayısal kısımda ise, modeller etrafındaki akış alanları, hız dağılımları ve balkon yüzeylerindeki basınç dağılımları Realizable $k-\epsilon$ türbülans modeli kullanılarak hesaplanmıştır. Model yüzeylerindeki basınç katsayıları dağılımları, farklı balkon yüksekliklerinin konumundan doğrudan etkilenmektedir. Farklı balkon yükseklikleri karşılaştırıldığında, en yüksek basınç katsayısı değerlerinin $h/d_1=3$ için elde edildiği, en kritik basınç katsayısı değerlerinin ise $h/d_1=4$ durumunda olduğu görülmüştür.

Anahtar Kelimeler: Balkon yüksekliği, hesaplamalı akışkanlar dinamiği (HAD), silindirik bina, basınç katsayısı, rüzgar tüneli.

1. INTRODUCTION

Due to the growing population and developing technology, the number of tall buildings constructed as an indicator of magnificence in large cities, often referred to as metropolises, has been gradually increasing. At the present time, some of the world's tallest structures are the Jeddah Tower with a height of 1000 m in Saudi Arabia (under construction), the Burj Khalifa in Dubai and the Shanghai Tower in China. Recent advancements in construction technology, application, and design techniques allow for the construction of such structures with unique and complex shapes.

The mega-tall structures, exceeding a height of 300 meters, exhibit different behavior from other structures in terms of aerodynamic characteristics and are usually influenced by lateral load stability because of wind loads [1]. The wind and earthquake loads are more influential than weight loads in tall structures, and they can be

damaged by strong winds or earthquakes due to their height. Such structural damage can result in loss of life and property [2]. Therefore, the adverse impacts of earthquake and wind-induced loads on such tall structures can be significantly reduced by various aerodynamic modifications to their outer designs. Studies in the literature cover a variety of configurations, including square and cylindrical structures, along with non-traditional plan-shaped tall structures such as triangular, cross, 'U', and 'L' shapes [3-7]. Additionally, implementing corner modifications proves highly effective in reducing aerodynamic loads on high-rise structures, as it minimizes flow separations at wind-facing corners and alters both the vortex structure and frequency of vortex formation behind the building [8-10]. The wind interactions around tall structures of varying shapes and heights are profoundly complex and have been studied for over five decades. Experimental

*Corresponding Author
e-posta : tekmilecurebal@ktu.edu.tr

procedures on this subject include wind tunnel testing and on-site measurements at full scale [11-18]. However, both methodologies are time-consuming, complex, costly, and limited to a finite number of spatial points [19]. Recently, Computational Fluid Dynamics (CFD) has been increasingly used as an alternative tool in wind engineering to examine the flow patterns around various models, such as buildings, airfoils, vehicles, turbine blades [20-23]. The principal advantage of CFD lies in its capability to simulate atmospheric boundary layer (ABL) flows with full-scale models within a computational domain. Moreover, CFD provides comprehensive insights into wind speeds, pressures, and concentrations throughout the entire flow field, whereas wind tunnel tests yield only limited measurements of these parameters [24]. In the literature, numerous studies have been carried out on the application of CFD for tall structures of varying shapes and heights. Baskaran and Kashef [25] assessed airflow conditions around different building configurations via CFD and emphasized the potential of CFD as a robust tool for generating detailed predictions of flow patterns around buildings. Lam and To [26] performed a comprehensive study on pedestrian-level wind (PLW) comfort around a row of tall buildings by using Re-Normalisation Group (RNG) $k - \varepsilon$ model. They reported that CFD results showed a $\pm 10\%$ agreement with experimental data in locations with high ground-level wind speeds, effectively capturing key features of the pedestrian-level wind environment around single tall buildings or the upwind building in a row, including high-speed corner streams, a standing vortex in front of the building, and a sheltered zone on the leeward side. Large eddy simulation (LES) and various revised $k - \varepsilon$ models results obtained around high-rise building model were compared by Tominaga et al. [27]. Their work revealed that the LES results with inflow turbulence demonstrated the best agreement with experimental results for velocity and turbulent energy distributions around the building, mainly due to its ability to accurately capture the periodic velocity fluctuations behind the building. The effect of surface roughness on the wind loads of an elliptical shaped high-rise structure was numerically investigated by Yan and Li [28]. The average drag force coefficient of the rough-walled tower was observed to increase significantly compared to the smooth-walled tower. Meng et al. [29] investigated the effects of geometric and computational parameters, such as approaching wind speed and direction, turbulence models, and grid type, on the pressure coefficient values of the Commonwealth Advisory Aeronautical Research Council (CAARC) building model. The results showed that phenomena such as fluid separation, vortex, wake effect, and reattachment varied with wind direction, causing significant changes in wind pressure and the turbulence model had a significant impact on the accuracy of the numerical results. Sharma et al. [30] computationally analyzed the separation ratio between two square cross-section tall buildings placed in tandem. The results indicated that in tandem arrangements, the

main building was shielded from flow by the upstream building, which consequently reduced wind forces and average wind speed at pedestrian level and the best wind conditions at pedestrian level was achieved with a minimum separation ratio. Sanyal and Dalui [31] examined the effect of different shapes and corner modifications of Y-plan-shaped buildings on wind loads and pressure distribution using ANSYS CFX. They concluded from the obtained data that the setback building model with rounded corners exhibited the best performance in reducing wind loads. Gerami and Kalehsar [32] evaluated interference effect of two CAARC tall building models using the LES turbulence model for different Reynolds numbers. The researchers concluded that a negative drag coefficient occurred in the opposite direction of the flow, and that the mean drag coefficient was lower for the principal building than for the isolated one, particularly in interference states. In an investigation of eight different building arrangements with inter-building angles ranging from 0° to 180° , Cürebal and Özmen [33] conducted a numerical analysis of velocity and pressure distributions within the flow field. Their findings indicate that the minimum dimensionless velocity value along the centerline of the passage occurs at an angle of 45° , whereas the maximum is observed at an angle of 135° . The effect of wind loads on various building models with regular and irregular shapes, under different corner configurations and wind incidence angles, was numerically investigated by Meena et al. [34]. It was found that, among all the models, the Y-shaped model with rounded corners produced the minimum base moment and the lowest drag coefficient. Alkhatib et al. [35] used finite element analysis to optimize wind loads on the Cayan Tower in Dubai, known for its complex structure. The findings indicated that the proposed approach effectively reduced along-wind and across-wind loads by 13.83% and 23.12%, respectively. Rajasekarababu et al. [36] assessed the computational performance and accuracy of six Unsteady Reynolds-Averaged Navier-Stokes (URANS) models in simulating wind flow characteristics around a setback tall building under open terrain wind conditions. They reported that the $k - \omega$ SST model was the most reliable choice for predicting mean flows and unsteady phenomena around setback building, as it required less computational time and resource utilization. The wind flows around tall buildings and the wind energy potential over flat roofs with different parapet heights were determined by Dai et al. [37]. This study emphasized that the separation of incoming flows from the parapet tips led to reversed low-velocity flows in the windward regions, which could reduce performance and increase the fatigue load on rooftop wind turbines. Additionally, velocity and turbulence intensity, influenced by normalized parapet height, were significantly dependent on roof location and wind angle.

The above literature review highlights that the main attention in the study of aerodynamic characteristics of buildings has been mostly given to configurations with

square and rectangular cross-sections, rather than circular sections, which entail notably complex flow fields. Therefore, there is a need to conduct more comprehensive studies regarding the evaluation of flow field and wind load on circular sections within high-rise buildings. Parameters such as the geometric features of the high-rise structures and their components (roof, balcony, etc.), positioning, wind speed, and wind direction directly affect the flow field around the structure and the pressure distributions on its surfaces. In this regard, the present study mainly focuses on examining the velocity distributions around circular cross-sectioned high-rise structures with and without balconies, aiming to obtain average pressure coefficients along the balcony surfaces based on balcony position and diameter.

2. EXPERIMENTAL APPARATUS AND PROCEDURE

The experimental study was conducted in an open-circuit wind tunnel in the Thermodynamics Laboratory of the Mechanical Engineering Department at Karadeniz Technical University. The dimensions of the tunnel test section are 457 mm (height) x 457 mm (width) x 2450 mm (length). Vortex generators, barrier, and roughness elements positioned at the entrance of the test section were used to simulate the atmospheric boundary layer. Figure 1 shows an illustrative diagram of the wind tunnel.

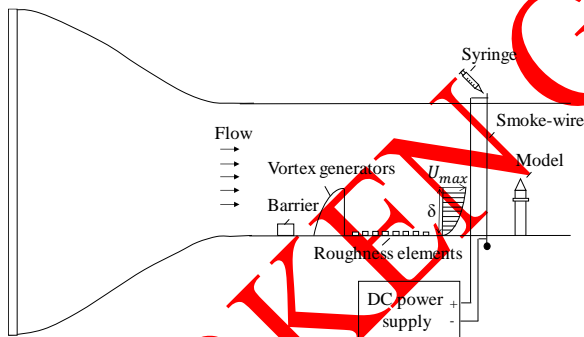


Figure 1. Illustrative diagram of the wind tunnel

Wind tunnel experiments aimed at assessing the wind effects around building models are typically conducted at free stream velocities ranging from 8 to 30 m/s [38]. Various studies have undertaken measurements at different free stream velocities to evaluate their impact on aerodynamic performance; these include Mo and Liu [39] at 8-11 m/s, Irtaza et al. [40] and Xia et al. [41] at 10 m/s, Uematsu and Isyumov [42] at 13 m/s, Kawai and Nishimura [43] at 15 m/s, and Kind [44] at 20 m/s. In the present study, a turbulent boundary layer of 150 mm thickness was obtained for a Reynolds number (Re) of 30000, calculated based on a free stream velocity of 15 m/s and the diameter of the model cylinder. The flow structures around the building model were investigated using the smoke-wire technique. A 0.2 mm thick

resistance wire was placed vertically in front of the models in the wind tunnel's test section, and paraffin vapor was continuously supplied along the wire by manually dripping the paraffin using a syringe. The wire was heated via DC current, causing the paraffin to vaporize through the Joule effect. The white vapor, which moved with the main flow, formed visual patterns that were captured by a video camera.

The dimensions of the experimental model structure are as follows: the cylinder's main body has a diameter of $d=30$ mm, the diameter of the balcony is $D_2=40$ mm, and the balcony height from the ground is $h_2=105$ mm, yielding an h_2/d ratio of 3.5 (Figure 2). The " h_2/d " ratio represents the relative height of the balcony from the ground (h_2) to the cylinder's main body diameter (d), which is fixed at 30 mm in this study. This ratio is a critical factor, as it signifies the proportional height of the balcony, which impacts the surrounding airflow characteristics and pressure distribution.

The blockage effect is a significant factor in wind tunnel tests, influencing the aerodynamic behavior of the model. A high blockage ratio can distort the surrounding flow and lead to inaccurate measurement results. In building aerodynamics studies, the ratio of the projected frontal (windward) area of the model to the cross-sectional area of the test region is referred to as the blockage effect, and it is recommended that a blockage ratio of less than 10% may be acceptable without correction to avoid flow choking [45]. In the current study, the blockage ratio was approximately 2.05%, which is well below the acceptable threshold. This ensures that the flow around the model remains largely undisturbed, allowing for accurate aerodynamic measurements.

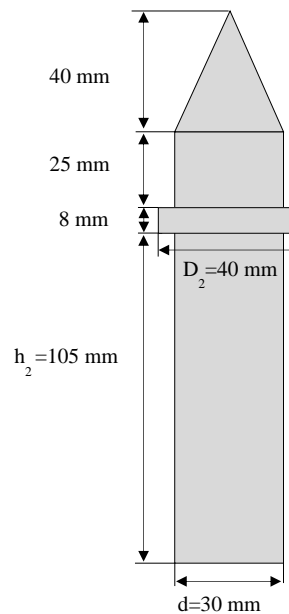


Figure 2. Dimensions of the experimental models

3. NUMERICAL STUDY

3.1. Mathematical Model and Solution Procedure

In the numerical part of the study, the continuity and Reynolds Averaged Navier-Stokes (RANS) equations were used to solve the flow field around the three-dimensional building models. The turbulent flow around the models was assumed to be steady-state and incompressible. The governing equations of incompressible flow are in the general form as follows:

$$\frac{\partial}{\partial x_i}(u_i) = 0 \quad (1)$$

$$\rho \frac{\partial}{\partial x_j}(u_i u_j) = -\frac{\partial p}{\partial x_i} + \frac{\partial}{\partial x_j} \left[\mu \left(\frac{\partial u_i}{\partial x_j} + \frac{\partial u_j}{\partial x_i} \right) - \frac{2}{3} \delta_{ij} \frac{\partial u_k}{\partial x_k} \right] + \rho \frac{\partial}{\partial x_j}(-\overline{u'_i u'_j}) + \rho g_i \quad (2)$$

The Realizable k- ϵ turbulence model, known for providing more precise outcomes in analyzing turbulence effects near the wall, was employed in solving the Reynolds-Averaged Navier-Stokes (RANS) equations [46]. Previous researchers have demonstrated that the Realizable k- ϵ models perform effectively in accurately and reliably modelling turbulent flows [29, 47, 48, 49]. The transport equations of incompressible flow for this turbulence model are defined as follows:

$$\rho \frac{\partial}{\partial x_j}(k u_j) = \frac{\partial}{\partial x_j} \left[\left(\mu + \frac{\mu_t}{\sigma_k} \right) \frac{\partial k}{\partial x_j} \right] + G_k + G_b - \rho \epsilon \quad (3)$$

$$\rho \frac{\partial}{\partial x_j}(\epsilon u_j) = \frac{\partial}{\partial x_j} \left[\left(\mu + \frac{\mu_t}{\sigma_\epsilon} \right) \frac{\partial \epsilon}{\partial x_j} \right] + \rho C_{1\epsilon} S_\epsilon - \rho C_{2\epsilon} \frac{\epsilon^2}{k + \sqrt{\nu \epsilon}} + C_{3\epsilon} \frac{\epsilon}{k} C_{3\epsilon} G_b \quad (4)$$

where turbulent kinetic energy productions due to average velocity gradients and buoyancy forces are indicated with the terms G_k and G_b . σ_k and σ_ϵ represent the turbulent Prandtl number for k and ϵ , respectively.

In the numerical simulation, conservation equations are discretized into algebraic equations using the finite volume method and solved using the ANSYS-FLUENT 18.0 software package. The dimensions of the flow field used for numerical solutions were based on the dimensions of the wind tunnel. The three-dimensional flow field and boundary conditions of the model are illustrated in Figure 3. The mean velocity and turbulence profiles, measured from the experimental study conducted by Özmen [50] in the wind tunnel, where the same atmospheric boundary layer was provided as

velocity inlet conditions for the computational domain (Figure 4).

Since the related model is suitable for the symmetric solution, it was created as half of the complete structure. For this reason, a symmetrical boundary condition was applied on one lateral surface. A pressure outlet boundary condition was specified for the outlet. A wall boundary condition was set for the other lateral surfaces, where a no-slip assumption holds. The Standard scheme was employed for pressure interpolation, and a second-order upwind scheme was chosen for discretizing other convection terms. The SIMPLEC algorithm was implemented to couple pressure and velocity. The enhanced wall treatment was used to resolve the boundary layer on the surfaces. The convergence criteria for Navier-Stokes equations were set to 1×10^{-5} .

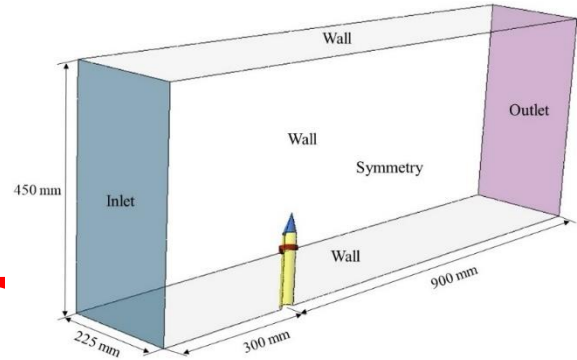


Figure 3. Flow field and boundary conditions

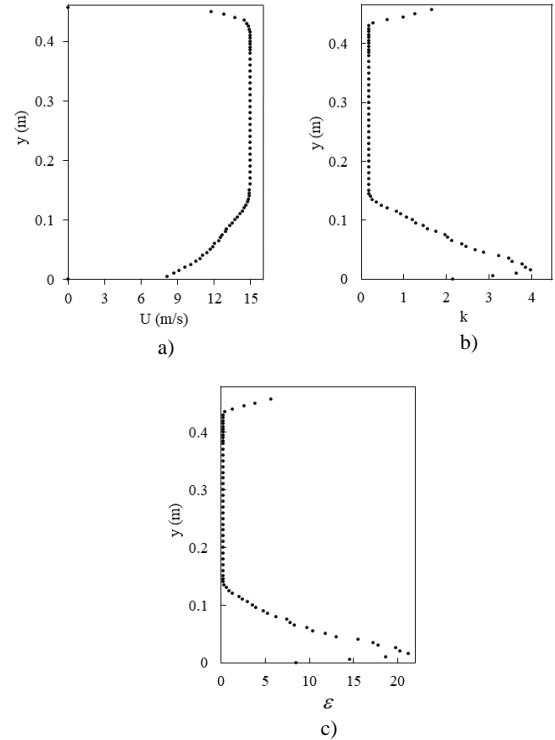


Figure 4. Profiles of (a) mean velocity, (b) turbulent kinetic energy and (c) turbulence dissipation rate

Numerical simulations were performed to evaluate the aerodynamic performance of the building model for three different height ratios: $h_1/d=3$, $h_2/d=3.5$, and $h_3/d=4$. Additionally, the balcony diameter was varied across three values: $D_1=35$ mm, $D_2=40$ mm, and $D_3=45$ mm.

These simulations aimed to analyze the combined effects of height and diameter adjustments on wind conditions. The dimensions of the building models used in the numerical study are illustrated in Figure 5.

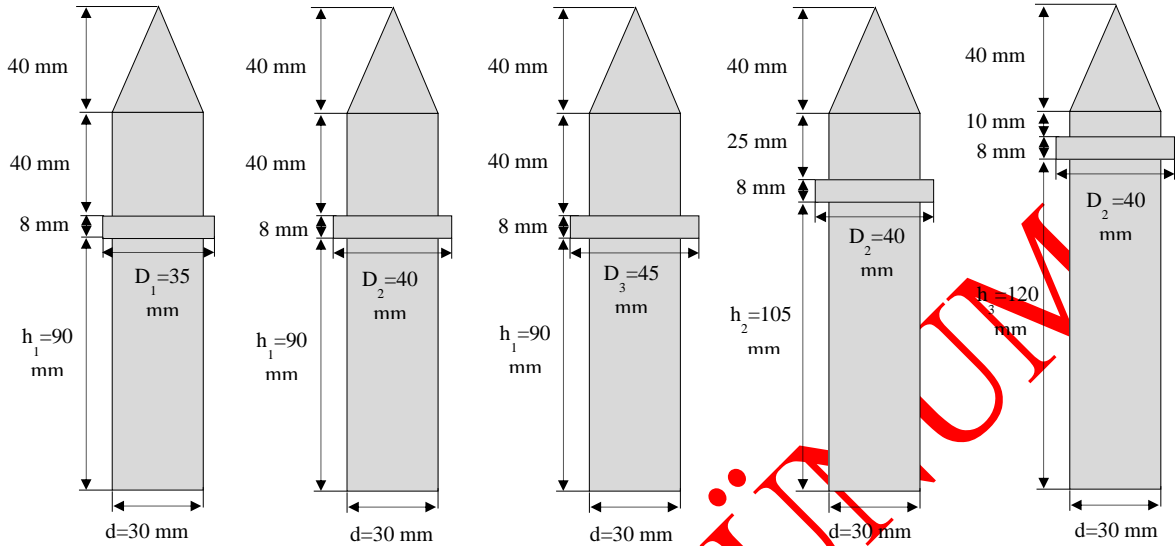


Figure 5. Dimensions of the models used in the numerical study

The mesh structure within the computational domain was generated using ICEM CFD software, creating a three-dimensional tetrahedral mesh structure for modeling turbulence characteristics (Figure 6). In order to accurately predict the characteristics of the viscous sublayer near the solid surfaces of the model, the mesh structure in these regions needs to be sufficiently refined [51-53]. For this reason, a fine mesh structure was used, particularly in proximity to solid surfaces, while a coarser mesh was preferred in other regions. A mesh independence study was performed at three different grids (approximately 560 thousand, 1.3 million, and 2.8 million) to compare the pressure coefficient values calculated along the middle axis of the model (Figure 7). It was observed that insignificant variations in the pressure coefficient values are obtained after 1.3 million cells. Thus, this cell structure was considered for further analysis, resulting in $y^+ \approx 2$ for the entire surface.

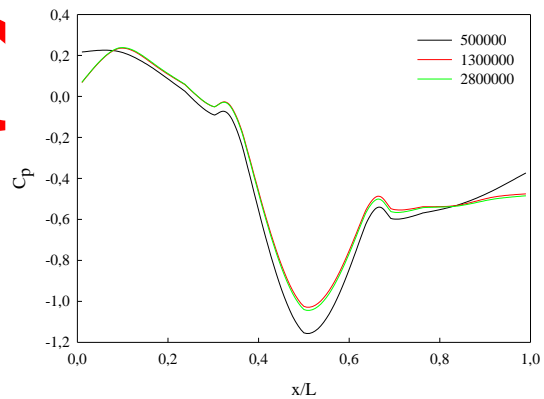


Figure 7. Effect of grid size on the solution

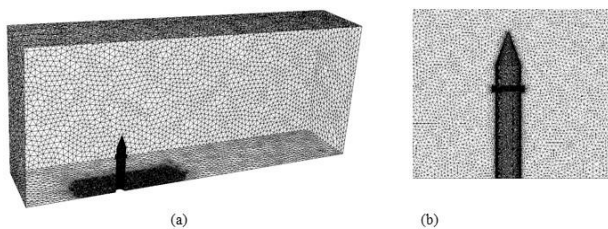


Figure 6. Illustration of mesh structure (a) computational domain, (b) model geometry

3.2. Validation of the Numerical Model

To validate the applied simulation approach, the experimental results of the study conducted by Ozmen and Aksu [46], which investigated the impact of different roof shapes on pressure distributions, were taken as a reference. For this purpose, the flow field around a cylindrical building model with a conical roof, one of the experimentally investigated models in the reference study, was numerically solved and compared with the experimental results. Figure 8 shows the pressure coefficient values calculated on the roof surfaces of the cylindrical building model with a conical roof as a comparison with the experimental data. It is seen that the pressure distribution calculated along the middle axis is found to be in agreement with the measurements, which confirms the numerical method.

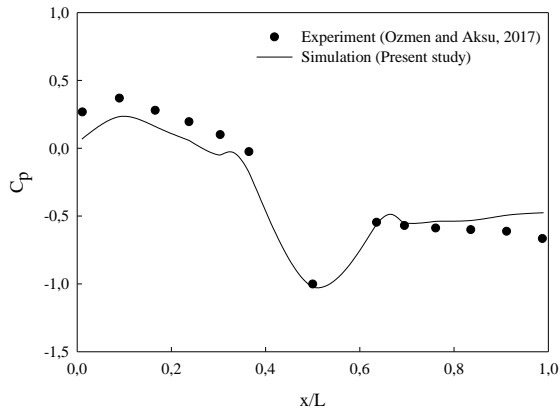


Figure 8. A comparison of the pressure distributions calculated on the roof surfaces along the middle axis with the experimental data

4. RESULTS AND DISCUSSION

4.1. Flow Visualization

Flow patterns around the model with a balcony height of 105 mm from its base ($h/d_1=3.5$), obtained using the smoke-wire technique and the Realizable $k-\epsilon$ turbulence model, are depicted in Figure 9. The incoming flow to the windward edge of the model impinges upon the surface and separates into two, as upstream and downstream from the stagnation point. The downstream flow generates a recirculation region within the balconies. On the other hand, the upstream flow separates from the roof's tip due to the relatively lower kinetic energy density compared to the pressure energy, leading to the development of a reverse flow region behind the model.

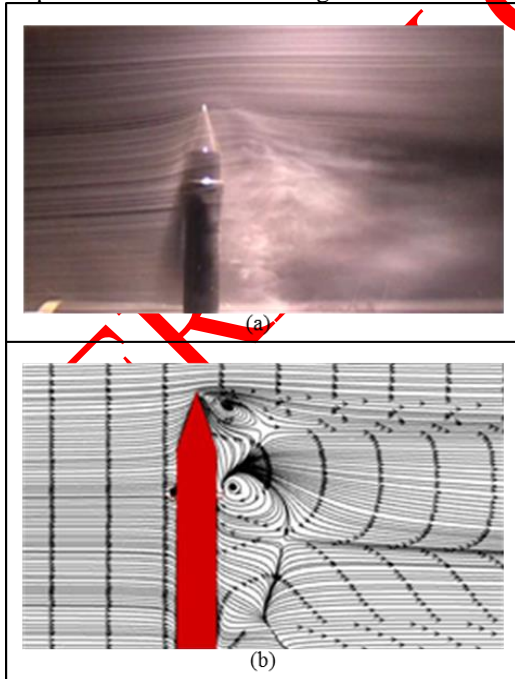


Figure 9. Flow patterns around the model: (a) Smoke-wire technique, (b) Realizable $k-\epsilon$ turbulence model

In order to examine the effect of the balcony position on the flow field, the balcony was positioned at three different heights. The flow patterns around the models for both the non-balcony and three different balcony heights are presented in Figure 10. Upon analyzing the flow patterns, it is evident that altering the balcony height does not lead to significant changes in the flow regions generated on the front and rear surfaces of the model. Nevertheless, when comparing the models with and without balconies, it becomes apparent that recirculation zones of varying sizes and positions emerge within the separated flow region behind the model. It is observed that as the balcony height increases, the vortices formed on the roof surface and within the balcony space move closer to each other.

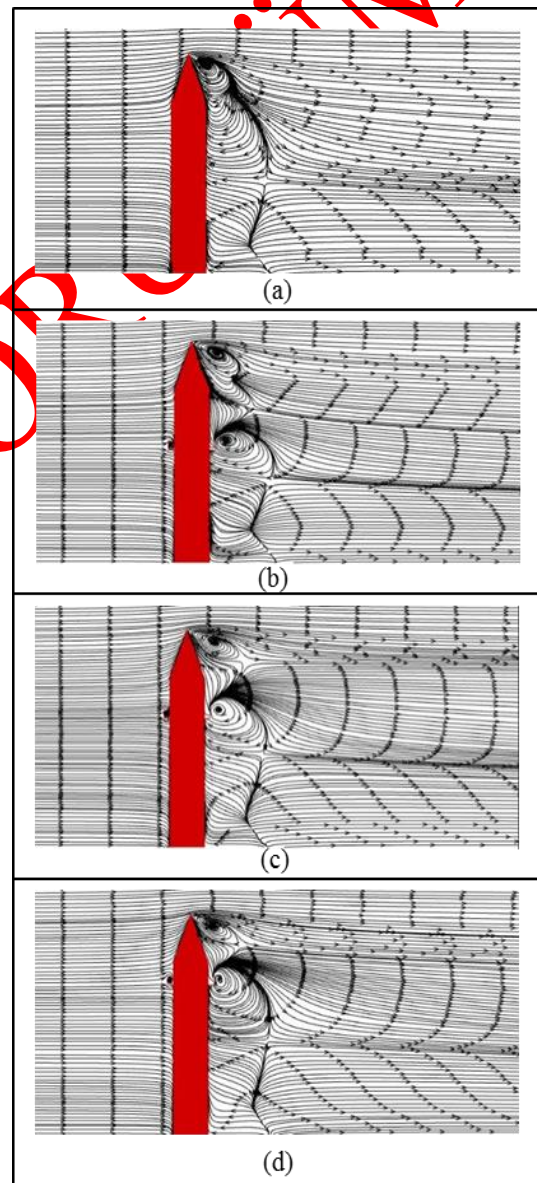


Figure 10. Flow patterns around models obtained for different balcony heights: (a) without balcony, (b) $h_1/d=3$, (c) $h_2/d=3.5$, (d) $h_3/d=4$

4.2. Velocity Distribution

Figure 11 presents the velocity contours at the vertical mid-plane of the models, encompassing both the non-balcony model and those with three distinct balcony heights. The incoming flow to the front surface of the model follows the roof surface, as expected. As seen, similar behavior is exhibited for all models examined. Moreover, the flow approaching the leading edge of the roof fails to adhere to the surface, resulting in corner streams with high wind speeds extending along the x-axis as the flow separates from the front roof edge. This separation causes reduced dimensionless velocity values on the roof and behind the model, where reverse flow regions emerge. Depending on the balcony's height position, the flow attaches to the surface due to the influence of vortices formed within the balcony space. Subsequently, the flow separates from this surface and merges with the ground, where the no-slip condition on the solid surface is effective.

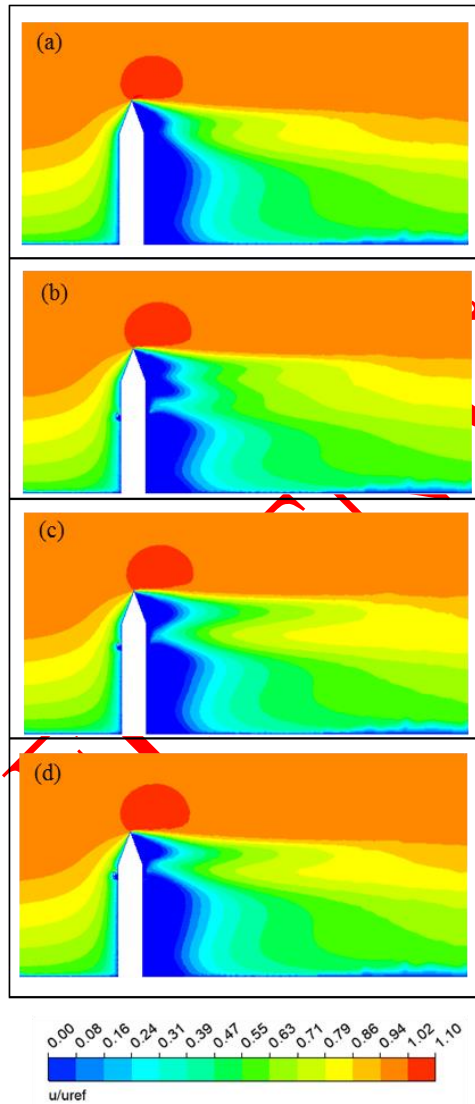


Figure 11. Velocity contours at the vertical mid-plane of the models (a) without balcony, (b) $h_1/d=3$, (c) $h_2/d=3.5$, (d) $h_3/d=4$

The velocity contours in the horizontal plane, calculated at different heights for the models with and without balconies, are compared in Figure 12. In all examined cases, it is clearly seen that the velocity values remain at low levels within the impact zones on the model's front surfaces. The flow, directed according to the model geometry starting from the front surface of the models, accelerates and creates a high-velocity region on the side surfaces. In contrast, the separated flow region with low-speed values is formed behind the models due to the flow being separated from the side surfaces. As illustrated in Figure 12 (b)-(d)-(f), the high-speed regions on the model's side surfaces expand while the regions of low-speed flow behind the model become narrower as the balcony height increases. Furthermore, it is observed that there is insignificant variation in the velocity contours obtained in the balcony space as the height increases. Upon comparing the velocity contours calculated at the same heights, it becomes apparent that the inclusion of a balcony in the model leads to a narrowing of the high-speed regions on the side surfaces, while the separated flow region extends behind the model. On the other hand, it should be noted that the low-speed regions formed on the model's front surfaces exhibit similar behaviors in terms of form and size.

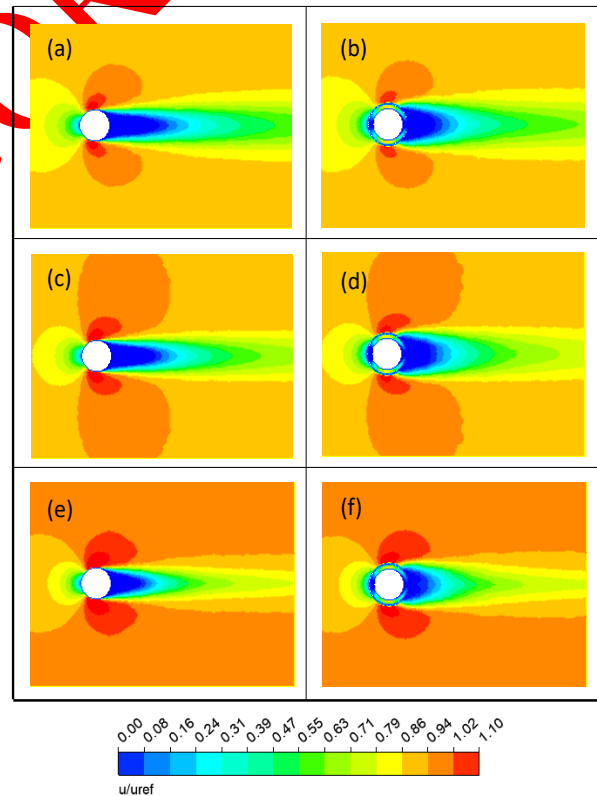


Figure 12. Velocity contours calculated for models with different heights (a) without balcony ($h_1/d=3$), (b) with balcony ($h_1/d=3$), (c) without balcony ($h_2/d=3.5$), (d) with balcony ($h_2/d=3.5$), (e) without balcony ($h_3/d=4$), (f) with balcony ($h_3/d=4$).

4.3. Pressure Distribution

Within the scope of the study, the pressure distributions on the surfaces of the examined models are evaluated in terms of dimensionless pressure coefficients. The definition of the dimensionless pressure coefficient is given by the following:

$$C_p = \frac{P - P_{ref}}{0.5\rho u^2} \quad (5)$$

For three different balcony heights, the variation of the pressure coefficient values calculated on the surfaces of the balcony in the windward region along the mid-axis of the model is shown in Figure 13. The positioning of the balcony at different heights directly affects the distribution of the pressure coefficient. As a general characteristic, it can be stated that the pressure coefficient values decrease with increasing balcony height. The positive pressure coefficients occur in the region where the incoming flow to the front surface of the model follows the A surface, while the negative pressure coefficients are formed in the separated flow region formed in the balcony space due to the suction effect. Additionally, the positive pressure coefficient values formed on the C surface indicate the presence of an impinging effect in this region. When the pressure coefficients on the D surface are evaluated, negative values are obtained due to the downstream flow directed from the stagnation point, and positive values are achieved because of the upstream flow effect. Furthermore, from the acquired pressure distributions on the surfaces of the balcony, it is seen that suction and impinging effects are more critical in the $h_3/d=4$ case than in the other cases. Taking into consideration the pressure distributions calculated on all balcony surfaces in the windward region, it is revealed that the best performance is observed in the case of $h_1/d=3$ case, where higher pressure values are occurred. In contrast, the other models experience more pronounced suction effects.

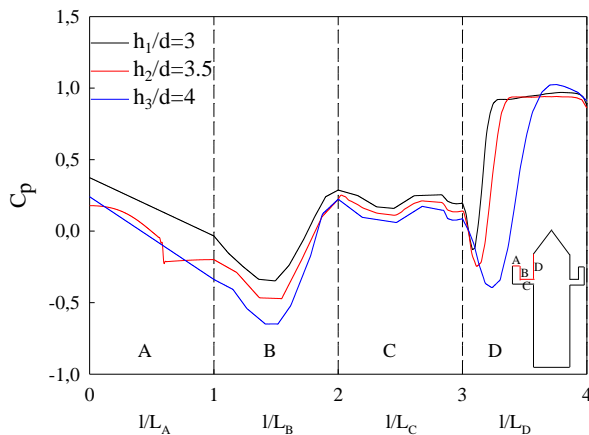


Figure 13. Variation of the pressure coefficient values calculated on the balcony surfaces in the windward region along the mid-axis for three different balcony heights

Figure 14 illustrates the variation of the pressure coefficient values calculated on the balcony surfaces in the leeward region along the mid-axis for three different balcony heights. Depending on the balcony heights, the pressure coefficient distributions on the balcony surfaces change significantly in the leeward region, with the maximum pressure coefficient values attained at $h_1/d=3$, where a notable reduction in suction effects is observed. Negative pressure coefficient values emerge on all balcony surfaces in the leeward region as a result of flow separation occurring at the roof tip. The negative effect of pressure coefficients, which exhibit peak values on the D' surface where separation begins, diminishes slightly towards the other surfaces, and it is observed that the most critical pressure coefficient value occurs in the case of $h_3/d=4$.

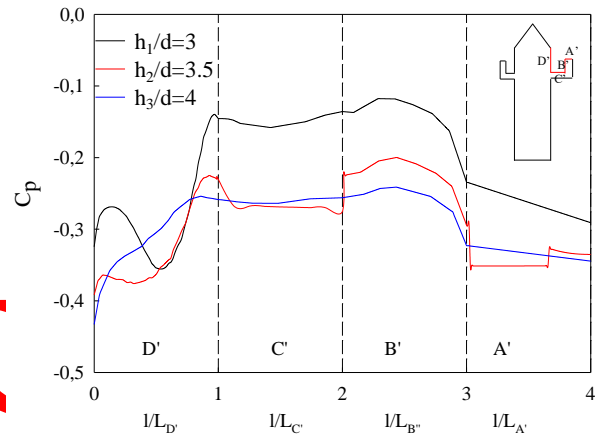


Figure 14. Variation of the pressure coefficient values calculated on the balcony surfaces in the leeward region along the mid-axis for three different balcony heights

When the pressure distributions calculated in the windward and leeward regions for different balcony heights are evaluated, it is observed that the maximum pressure coefficient values occur in the case of $h_1/d=3$. At this height, where the best performance is achieved, the effect of balcony diameter on the pressure coefficient is examined by considering three different balcony diameters ($D_1=35$ mm, $D_2=40$ mm, $D_3=45$ mm). The variation of pressure coefficient values calculated on the balcony surfaces along the mid-axis in the windward and leeward regions for these three different balcony diameters are illustrated in Figure 15. As depicted in the Figure 15(a), the pressure distributions calculated on all balcony surfaces in the windward region decrease as the balcony diameter increases. In addition to this, the corresponding pressure coefficients indicate that surface B has the most critical suction effect. It appears that the most critical minimum pressure coefficient is calculated on the balcony surfaces of the model with a diameter of $D_3=45$ mm as an approximate value of -0.61. Further, the highest suction effect is observed on Surface D' in the leeward region and is not affected by the change in the balcony diameter (Figure 15(b)). For all balcony diameters, the most critical pressure coefficient values

calculated on this surface are determined as approximately -0.35. This indicates that the leeward region is less critical in terms of suction effect compared to the windward region. The findings reveal that the model with a balcony diameter of $D_1=35$ mm is more effective in improving the critical suction effect.

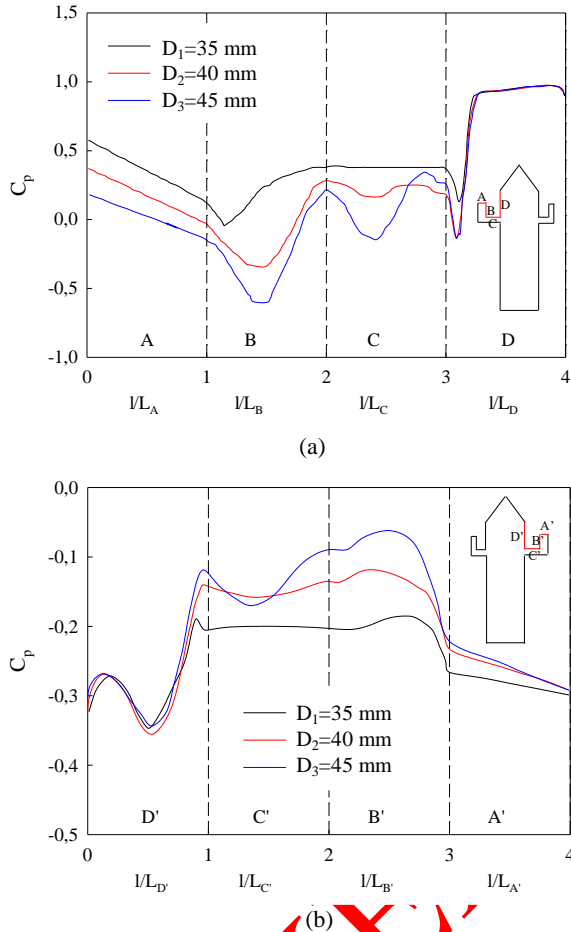


Figure 15. Variation of the pressure distributions calculated on the balcony surfaces along the middle axis of the model for three different balcony diameters (a) windward region, (b) leeward region

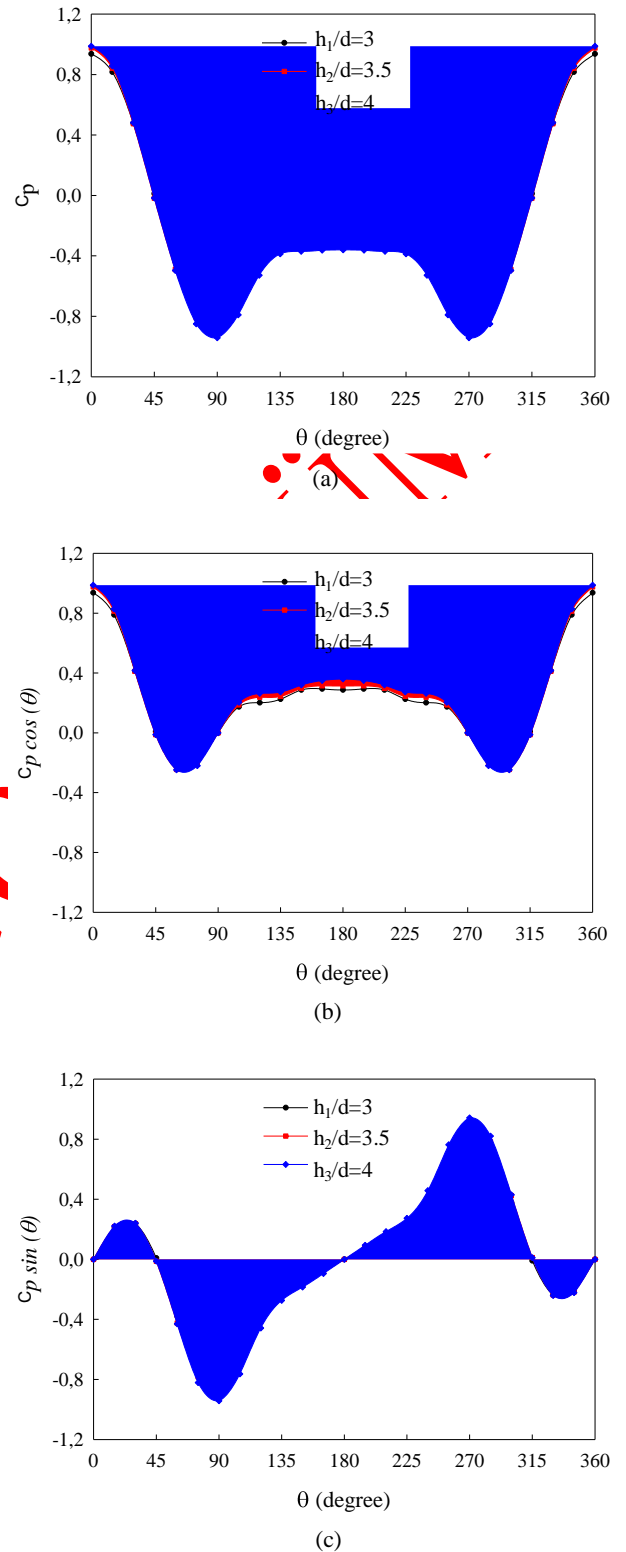


Figure 16. Pressure distributions and their components calculated around the circumference of the balcony surface at the mid-axis for three different balcony heights (a) pressure coefficient, (b) drag component, (c) lift component

The drag and lift coefficients of the model with different balcony heights are also evaluated. There are a variety of methods to assess these coefficients. In this study, they are derived through the integration of the calculated pressure distribution across the balcony surface. The drag coefficient (C_d) and the lift coefficient (C_l) calculations are described in Equations (6) and (7), respectively.

$$C_d = \frac{1}{2} \int_0^{2\pi} C_p \cos(\theta) d\theta \quad (6)$$

$$C_l = -\frac{1}{2} \int_0^{2\pi} C_p \sin(\theta) d\theta \quad (7)$$

Pressure distributions and their components calculated around the circumference of the balcony surface at the mid-axis are shown in Figure 16. Comparisons are performed considering the different balcony heights. The pressure coefficient's drag component is represented as $C_p \cos(\theta)$, while its lift component is expressed as $C_p \sin(\theta)$. The calculated average values of drag coefficient (\bar{C}_d), corresponding to increasing balcony heights, are obtained as 0.2448, 0.2537, and 0.2677, respectively. It can be observed that there are no significant changes in drag coefficients when compared to values associated with various balcony heights. The lift coefficient is also determined using the same procedure, resulting in a value of $\bar{C}_l = 0$.

5. CONCLUSIONS

In this study, the flow patterns around circular cross-sectioned high-rise structures, the velocity distribution, and the pressure coefficient obtained on the surfaces of the balcony are evaluated. The results obtained for three different balcony heights and diameters are compared with the model without a balcony, and the following main outcomes are achieved.

- 1) For the balcony model with $h_2/d=3.5$, the flow field image computed by the Realizable $k-\epsilon$ turbulence model is generally consistent with the photograph of flow visualization. The incoming flow to the front surface of the model separates from the roof's tip and creates a reverse flow region behind the model.
- 2) When the flow patterns of the balcony located at different heights are examined, no significant changes are observed in the flow regions formed on the front and rear surfaces of the model.
- 3) The velocity distributions calculated behind the model show that the flow attaches to the surface with the effect of the vortices formed in the balcony space, depending on the position of the balcony height.
- 4) As the height of the balcony increases, the high-speed regions on the side surfaces of the model

extend, while the low-speed regions behind the model become narrow for all the configurations considered.

- 5) The pressure coefficient distributions are directly affected by the position of different balcony heights. The pressure distributions calculated on the surfaces of balcony in the windward region along the mid-axis of the model decrease as the height increases.
- 6) The maximum pressure coefficient values are achieved for $h_1/d=3$, and the minimum pressure coefficient values are observed for $h_3/d=4$ on all balcony surfaces in the windward and leeward regions.
- 7) The model with a balcony diameter of $D_1=35$ mm is more effective in improving the critical suction effect in the change of the pressure coefficient values computed for three different balcony diameters.

DECLARATION OF ETHICAL STANDARDS

The author(s) of this article declare that the materials and methods used in this study do not require ethical committee permission and/or legal-special permission.

AUTHORS' CONTRIBUTIONS

Aleyna AĞIRMAN KALCA: Simulation, validation, investigation, writing – original draft.

Tekmile ÇÜREBAL: Simulation, validation, investigation, writing – original draft and revision.

Yücel ÖZMEN: Conceptualization, visualization, writing – original draft and revision.

CONFLICT OF INTEREST

There is no conflict of interest in this study.

REFERENCES

- [1] Taranath B. S., "Tall building design: steel, concrete and composite systems", *CRC Press*.
- [2] Rahman A., Fancy S. F. and Bobby S. A., "Analysis of drift due to wind loads and earthquake loads on tall structures by programming language c", *International Journal of Scientific & Engineering Research*, 3(6), (2012).
- [3] Gomes M. G., Rodrigues A. M. and Mendes P., "Experimental and numerical study of wind pressures on irregular-plan shapes", *Journal of Wind Engineering and Industrial Aerodynamics*, 93(10): 741-756, (2005).
- [4] Kumar E. K., Tamura Y., Yoshida A., Kim Y. C. and Yang, Q., "Journal of wind engineering experimental investigation on aerodynamic characteristics of various triangular-section high-rise buildings", *Journal of Wind Engineering and Industrial Aerodynamics*, 122: 60-68, (2013).
- [5] Mukherjee S., Chakraborty S., Dalui S. K. and Ahuja A. K., "Wind-induced pressure on "Y" plan shape tall building", *Wind and Structures*, 19(5): 523-540, (2014).
- [6] Kumar D. and Dalui, S. K., "Effect of internal angles between limbs of cross plan shaped tall building under

- wind load”, *Wind and Structures*, 24(2): 95-118, (2017).
- [7] Xu X., Yang Q., Yoshida A. and Tamura Y., “Characteristics of pedestrian-level wind around super-tall buildings with various configurations”, *Journal of Wind Engineering and Industrial Aerodynamics*, 166: 61-73, (2017).
- [8] Ozmen Y. and Kaydok T., “Numerical investigation of turbulent flow over a high-rise building with square cross-section area”, *KSU Journal of Engineering Sciences*, 17(2): 15-25, (2014).
- [9] Mittal H., Sharma A. and Gairola A., “Numerical simulation of pedestrian level wind flow around buildings: effect of corner modification and orientation”, *Journal of Building Engineering*, 22: 314-326, (2019).
- [10] Sanyal P. and Dalui S. K., “Effect of corner modifications on ‘Y’ plan shaped tall building under wind load”, *Wind and Structures*, 30 (3): 245-260., (2020).
- [11] Maruyama T., Taniguchi T., Okazaki M. and Taniike Y., “Field experiment measuring the approaching flows and pressures on a 2.4 m cube”, *Journal of Wind Engineering and Industrial Aerodynamics*, 96: 1084-1091, (2008).
- [12] Irwin P., “Wind engineering challenges of the new generation of super-tall buildings”, *Journal of Wind Engineering and Industrial Aerodynamics*, 97: 328-334, (2009).
- [13] Tsang C. W., Kwok K. C. S. and Hitchcock P.A., “Wind tunnel study of pedestrian level wind environment around tall buildings: Effects of building dimensions, separation and podium”, *Building and Environment*, 49: 167-181, (2012).
- [14] Tanaka H., Tamura Y., Ohtake K., Nakai M. and Kim Y. C., “Experimental investigation of aerodynamic forces and wind pressures acting on tall buildings with various unconventional configurations”, *Journal of Wind Engineering and Industrial Aerodynamics*, 107–108: 179-191, (2012).
- [15] Bandi E. K., Tamura Y., Yoshida A., Kim Y. C. and Yang Q., “Experimental investigation on aerodynamic characteristics of various triangular section high-rise buildings” *Journal of Wind Engineering and Industrial Aerodynamics*, 122: 60-68, (2013).
- [16] Yan B. and Li Q. S., “Wind tunnel study of interference effects between twin super-tall buildings with aerodynamic modifications”, *Journal of Wind Engineering and Industrial Aerodynamics*, 156: 129-145, (2016).
- [17] Nagar S. K., Raj R. and Dev N., “Experimental study of wind-induced pressures on tall buildings of different shapes”, *Wind and Structures*, 31(5): 441-453, (2020).
- [18] Chen F. B., Liu H. M., Chen W., Shu Z. R., Li Y., Li Q. S. and Han Y., “Characterizing wind pressure on CAARC standard tall building with various façade appurtenances: An experimental study”, *Journal of Building Engineering*, 59: 105015, (2022).
- [19] Stathopoulos T., “Computational wind engineering: past achievements and future challenges”, *Journal of Wind Engineering and Industrial Aerodynamics*, 67-68: 509-532, (1997).
- [20] Yang X., Hu Y., Gong Z., Jian J. and Liu Z., “Numerical study of combined drag reduction bases on vortex generators and riblets for the ahmed body using iddes methodology”, *Journal of Applied Fluid Mechanics*, 15(1): 193-207, (2022).
- [21] Potsis T., Tominaga Y. and Stathopoulos T., “Computational wind engineering: 30 years of research progress in building structures and environment”, *Journal of Wind Engineering and Industrial Aerodynamics*, 234: 105346, (2023).
- [22] Bao T., Hu J., Huang C. and Yu Y., “Smoothed particle hydrodynamics with κ - ϵ closure for simulating wall-bounded turbulent flows at medium and high Reynolds numbers”, *Physics of Fluids*, 35(8): 085114, (2023).
- [23] Li Y., Yang S., Feng F. and Tagawa K., “A review on numerical simulation based on CFD technology of aerodynamic characteristics of straight-bladed vertical axis wind turbines”, *Energy Reports*, 9: 4360-4379, (2023).
- [24] Franke J., Hirsch C., Jensen G., Krus H. W., Miles S. D., Schatzmann M., Westbury P. S., Wise J. A. and Wright N., “Recommendations on the use of CFD in wind engineering”, *In Proceedings of the International Conference on Urban Wind Engineering and Building Aerodynamics*, (2004).
- [25] Baskaran A. and Kashef A., “Investigation of air flow around buildings using computational fluid dynamics techniques”, *Engineering Structures*, 18(11): 861-873, (1996).
- [26] Lam, K. M. and To A. P., “Reliability of numerical computation of pedestrian-level wind environment around a row of tall buildings”, *Wind and Structures*, 9(6): 473-492, (2006).
- [27] Tominaga Y., Mochida A., Murakami S. and Sawaki S., “Comparison of various revised k- ϵ models and LES applied to flow around a high-rise building model with 1:1:2 shape placed within the surface boundary layer” *Journal of Wind Engineering and Industrial Aerodynamics*, 96: 389–411, (2008).
- [28] Yan B. W. and Li Q. S., “Detached-eddy and large-eddy simulations of wind effects on a high-rise structure”, *Computers and Fluids*, 150: 74–83, (2017).
- [29] Meng F. Q., He B. J., Zhu J., Zhao D. X., Darko A. and Zhao, Z. Q., “Sensitivity analysis of wind pressure coefficients on CAARC standard tall buildings in CFD simulations”, *Journal of Building Engineering*, 16: 146-158, (2018).
- [30] Sharma A., Mittala H. and Gairola A., “Detached-eddy simulation of interference between buildings in tandem arrangement”, *Journal of Building Engineering*, 21: 120-140, (2019).
- [31] Sanyal P. and Dalui S. K., “Comparison of aerodynamic coefficients of various types of Y-plan-shaped tall buildings”, *Asian Journal of Civil Engineering*, 21: 1109–1127, (2020).
- [32] Germi M. S. and Kalehsar H. E., “Numerical investigation of interference effects on the critical wind velocity of tall buildings”, *Structures*, 30: 239-252, (2021).
- [33] Cürebal T. and Özmen, Y., “Açılı konumlandırılmış iki bina arasındaki açının hız ve basınç dağılımı üzerine etkisinin sayısal incelenmesi”, *Politeknik Dergisi*, 25(1): 361-371, (2022).
- [34] Meena R. K., Raj R. and Anbukumar S., “Effect of wind load on irregular shape tall buildings having different corner configuration”, *Sādhanā*, 47: 126, (2022).
- [35] Alkhatib F., Kasim N., Goh W. I., Shafiq N., Amran M., Kotov E. V. and Albaom M. A., “Computational

- aerodynamic optimization of wind-sensitive irregular tall buildings”, *Buildings*, 12(7): 939, (2022).
- [36] Rajasekarababu K. B., Vinayagamurthy G. and Selvi Rajan S., “Evaluation of CFD URANS Turbulence Models for the Building under Environmental Wind Flow with Experimental Validation”, *Journal of Applied Fluid Mechanics*, 15(5): 1387-1401, (2022).
- [37] Dai S. F., Liu H. J. and Peng H. Y., “Assessment of parapet effect on wind flow properties and wind energy potential over roofs of tall buildings”, *Renewable Energy*, 199: 826-839, (2022).
- [38] Ozmen Y., “Experimental and theoretical investigation of the wind effects on buildings with different roof types and slopes”. Doctoral Thesis, K.T.Ü Graduate School of Natural and Applied Sciences, (2006).
- [39] Mo Z. and Liu C.H., “A wind tunnel study of ventilation mechanism over hypothetical urban roughness: The role of intermittent motion scales”, *Building and Environment*, 135: 94-103, (2018).
- [40] Irtaza H., Beale R.G., Godley M.H.R. and Jameel A., “Comparison of wind pressure measurements on Silsoe experimental building from full-scale observation, wind-tunnel experiments and various CFD techniques”, *International Journal of Engineering, Science and Technology*, 5 (1): 28-41, (2013).
- [41] Xia Q., Liu X., Niu J. and Kwok, K.C.S., “Effects of building lift-up design on the wind environment for pedestrians”, *Indoor and Built Environment*, 26(9): 1214-1231, (2015).
- [42] Uematsu Y. and Isyumov N., “Wind pressures acting on low-rise buildings”, *Journal of Wind Engineering and Industrial Aerodynamics*, 82: 1-25, (1999).
- [43] Kawai H. and Nishimura G., “Characteristics of fluctuating suction and conical vortices on a flat roof in oblique flow”, *Journal of Wind Engineering and Industrial Aerodynamics*, 60: 211-225, (1996).
- [44] Kind R.J., “Worst Suctions Near Edges of Flat Rooftops on Low-Rise Buildings”, *Journal of Wind Engineering and Industrial Aerodynamics*, 25: 31-47, (1986).
- [45] Kirrane P.P. and Steward S.J., “The effect of blockage on shear flow in the wind tunnel”, Doctoral Thesis, University of Bristol Department of Aeronautical Engineering, (1978).
- [46] Ozmen Y. and Aksu E., “Wind pressures on different roof shapes of a finite height circular cylinder”, *Wind and Structures*, 24 (1): 25-41, (2017).
- [47] Tanürün H. E., Akın A. G. and Acır A., “Rüzgâr türbinlerinde giriş yapısının performansa etkisinin sayısal olarak incelenmesi”, *Politeknik Dergisi*, 24 (3): 1219–1226, (2021).
- [48] Soydan N.G., Şimşek O. and Aköz M.S., “Köprü ayağı etrafındaki türbülanslı akımın sayısal ve deneysel analizi”, *Politeknik Dergisi*, 21(1): 137–147, (2018).
- [49] Blocken B., Janssen W.D. and van Hooff, T., “CFD simulation for pedestrian wind comfort and wind safety in urban areas: General decision framework and case study for the Eindhoven University campus”, *Environmental Modelling & Software*, 30: 15-34, (2012).
- [50] Ozmen Y., “Effect of parapets to pressure distribution on flat top of a finite cylinder”, *Wind and Structures*, 17(5): 465-477, (2013).
- [51] Franke J., Hellsten A., Schunzen H. and Carissimo B., “Best practice guideline for the CFD simulation of flows in the urban environment: Cost Action 732 Quality assurance and improvement of microscale meteorological models”, (2007).
- [52] Dagnew A. K., Bitsuamalk G. T. and Merrick R., “Computational evaluation of wind pressures on tall buildings”, *11 th Americas Conference on Wind Engineering*, San Juan, Puerto Rico, (2009).
- [53] Mohammadpour R., Ghani A. A. and Azamathulla H. M., “Numerical modelling of 3D flow on porous broad crested weirs”, *Applied Mathematical Modelling*, 37 (22): 9324-9337, (2013).